Available online at www.ijournalse.org

Emerging Science Journal

(ISSN: 2610-9182)

Vol. 6, No. 3, June, 2022

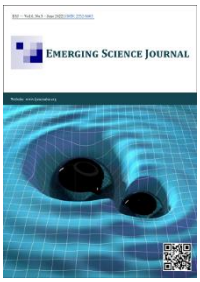

Effect of Turbocharger Compression Ratio on Performance of the Spark-Ignition Internal Combustion Engine

Saad S. Alrwashdeh [1, 2*], Ala'a M. Al-falahat [1], Talib K. Murtadha [1]

[1] *Mechanical Engineering Department, Faculty of Engineering, Mutah University, P.O Box 7, Al-Karak 61710, Jordan.*

[2] *Materials Science and Energy Lab, MSEL. Mutah University, P.O Box 7, Al-Karak 61710, Jordan.*

Abstract

Internal Combustion Engines (ICE) are one of the most important engineering applications that operate based on the conversion of chemical energy from fuel into thermal energy as a result of direct combustion. The obtained thermal energy is then turned into kinetic energy to derive various means of transportation, such as marine, air, and land vehicles. The efficiency of ICE today is considered in the range of the intermediate level, and various improvements are being made to enhance its efficiency. The turbocharger can support the ICE, which works by increasing the pressure in the engine to enhance its efficiency. In this investigation, the effect of the turbocharger pressure on ICE performance was studied in the range of 2 to 10 bar. It was found that the increase in turbocharger pressure enhanced the pressure inside the engine, positively affecting engine efficiency indicators. Therefore, the increase in turbocharger pressure is directly proportional to the ICE efficiency.

Keywords:

Internal Combustion Engines;
Engine Performance;
Turbocharger.

Article History:

Received:	06	December	2021
Revised:	23	February	2022
Accepted:	11	March	2022
Available online:	19	April	2022

1- Introduction

Energy is one of the most important issues in sustainability, as the presence of its sources is an indicator of the strength and stability of its location [1-3]. Energy sources are now depleting, resulting in conflicts between different countries as well as many crises and disasters [4-6]. In this regard, the search for alternative energy sources has become of great importance. In this context, renewable energy sources such as the sun and wind are promising candidates to resolve complex energy problems [7-9].

Energy problems are not limited to their sources and the discovery of alternatives to traditional sources, as the optimal use of energy sources, whether traditional or renewable, at the highest efficiency and within the best international standards and practices is also highly crucial [10-12]. Here, the importance of efficient energy systems and optimal consumption is one of the essential issues [13, 14]. Studies in this field can be divided into two main classes [15-21]. While the first group involves the search for alternative sources of energy with a special focus on renewable energy sources such as solar, wind, geothermal, tidal energy, and fuel cells [22-24], the second group deals with the issue of rationalizing consumption and increasing the efficiency of various energy systems [1, 12, 25].

The combustion engine is one of the most important and widely employed devices in various industries [26-28]. The chemical energy of the fuel is converted into thermal energy in a combustion engine through direct combustion. The obtained thermal energy is then transformed into mechanical energy to be used for various purposes [29, 30]. Depending

* **CONTACT**: saad.alrwashdeh@mutah.edu.jo

DOI: http://dx.doi.org/10.28991/ESJ-2022-06-03-04

on the place of fuel-burning, combustion engines are classified into two types: external and internal combustion engines. The former is the oldest type and depends on completing the process of burning the fuel in a specific area and then transferring energy to be used in another place [31]. While the latter relies on completing the burning of the fuel process and using it in the same place. The internal combustion engine is the latest and most widely used type. Several advantages such as simplicity of mechanics, higher power per working cycle, low cost, and efficiency make the internal combustion engine the best candidate [32-34].

Numerous studies have addressed the development of combustion engines, especially the internal type. Jafari et al. (2020) [35] developed an active thermo-atmospheric combustion concept. Negoro et al. (2013) [36] tried to improve Toyota cars by controlling the combustion toward an auto-ignition to ensure the stabilization inside the internal combustion engines. Doppalapudi et al. (2021) [37] analyzed the effect of thermal stress on some parts of the internal combustion engines such as the piston, connecting rods, and pins; they found that the pressure on the pistons of the engine plays a major role in transforming the engine load from the combustion chamber which lies inside the cylinder to the crankshaft of the engine through the connecting rod.

Concerning the development of the engines, 1862 Alphonse described an efficient four-stroke cycle engine and the connection between the operating conditions through investigating the ignition system with high pressure during the compression cycle and the relation between the compression cycles by increasing the volume of the burned mixture [38]. Numerous works addressed the design and improvement of internal combustion engines to improve their efficiency and performance. Examples of improvements are camshaft improvements, fuel injection system improvements, and improvements to the design of the combustion chambers. The cylinder balance is the main factor in the reduction of the torsional vibrations that comes from the unbalanced cylinders in the engines. In this frame, the injectors of the fuel cylinder are automated to control the injection times, through controlling the dynamic loads which aid in a uniform distribution of the mechanical strain all over the internal combustion engine parts [39-41].

Fuel injection systems are considered one of the most important support systems in internal combustion engines [42-44]. These systems have faced many developments and improvements. The first engines had direct-flow and traditional injection systems which were then developed into systems with direct and indirect injection systems to ensure supplying the sufficient amount of fuel to run the engines at the highest efficiency and fuel economy. In this work, the performance of the spark-ignition internal combustion engines is investigated based on a turbocharger with different pressure compression ratios starting from 2 to 10 bars. The investigation is aimed to assess the correlation between the pressure ratio of the turbocharger and the ICE performance.

2- Theoretical Background

Figure 1 indicates the basics of the engine cylinder in which combustion takes place. The energy conversion process starts due to the linear motion that results from combustion inside it. The engine cylinder includes a piston, connecting rods, crank, and crankshaft. The process of the energy conversion starts from the fuel injection point to the cylinder where the piston begins to move from the top dead center (TDC) to the bottom dead center (BDC) what is known as the intake stroke followed by the compression process which is a reversible motion of the piston from BDC to TDC. With increasing the pressure, the spark comes to make the firing to let the piston expand from the TDC to BDC in what is known as the expansion stroke. Finally, the piston comes to its origin to start over again with what is known as exhaust stroke. All these steps complete the conversion process of the energy [26].

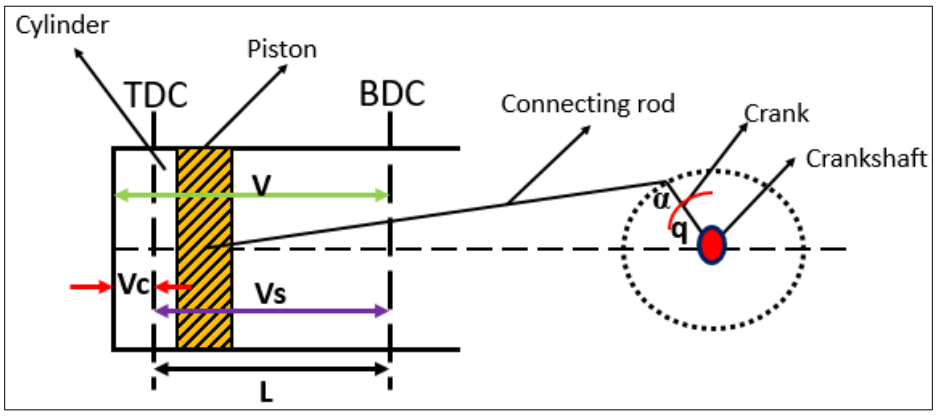

Figure 1. The basics of the engine cylinder

The geometry of the piston, connecting rods, and the crank is shown in Figure 2 with some dimensions indicating the geometry of the energy conversion of the engine.

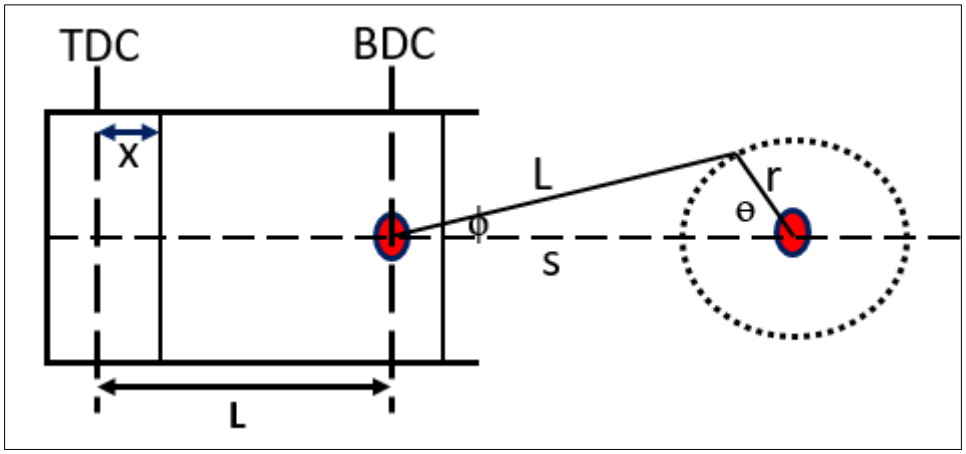

Figure 2. Geometry of the piston

$$L.sin\emptyset = a.sin \tag{1}$$

$$sin\ \emptyset = \frac{a}{L}.sin\theta \tag{2}$$

where, Ø is angle of the connecting rod relative to the center line of the cylinder, θ is crank angle from the TDC position, a is crank radius, and L is connecting rod length.

$$cos\emptyset = \sqrt{1 - sin^2\emptyset} \tag{3}$$

$$cos\emptyset = \sqrt{1 - \frac{a^2}{L^2}sin^2\theta} \tag{4}$$

The distance s between the crank axis and the wrist pin axis can be determined by:

$$s = a.cos\theta + \sqrt{L^2 - a^2.sin^2\theta} \tag{5}$$

The piston displacement from the TDC position is given by:

$$s = a.cos\theta + \sqrt{L^2 - a^2.sin^2\theta} \tag{6}$$

Instantaneous piston speed:

$$U_p = 2\pi N\left[a.sin\theta + \frac{a^2 sin\theta cos\theta}{\sqrt{L^2 - a^2 sin^2\theta}}\right] \tag{7}$$

Mean piston speed:

$$\frac{U_p}{\overline{U_p}} = \frac{\pi}{L}sin\theta\left[1 + \frac{cos\theta}{\sqrt{R^2 - sin^2\theta}}\right] \tag{8}$$

The power developed inside the cylinder of the engine is called indicated power. While the actual power available from the crankshaft is called the break power. The frictional power is the difference between the indicated and break powers. Figure 3 shows the work algorithm, which started from determining the type of engine (an internal combustion engine) that works by a spark. Then, the effect of different pressure ratios (2-10 bar at 2-bar intervals) was assessed by using a turbocharger. The efficiency parameters and the effect of increasing the pressure inside the engine were also explored. The work methodology of this investigation relied on the selection of the internal combustion engine operating with spark. The turbocharger served as an auxiliary factor. The work began by changing the supplied pressure ratio of the engine using a turbocharger (2-10 bar); then, a wide range of performance indicators was studied, including the engine power, friction power, fuel consumption rate, temperature, and pressure. At the end of each stage, an extensive comparison was made based on every new compression ratio. The relationship between the compression ratio supplied by the turbocharger to the engine and the engine efficiency was also extracted as the final result.

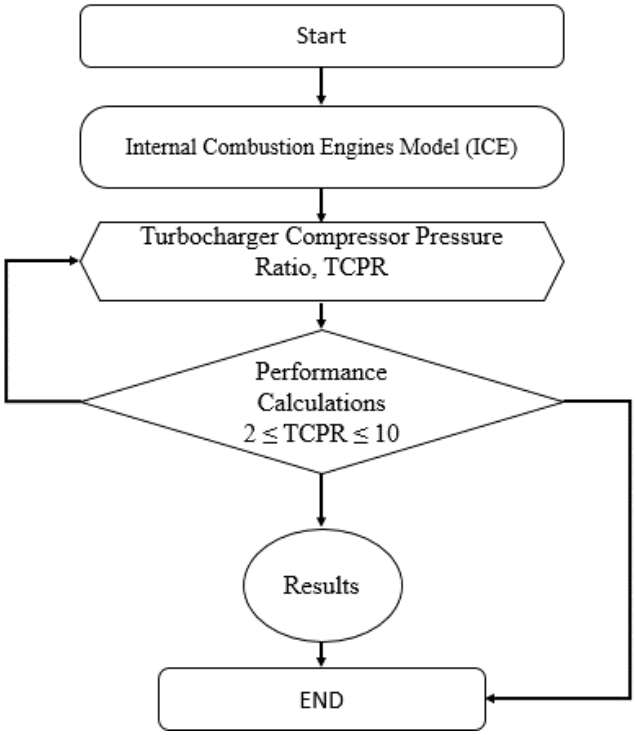

Figure 3. Methodology flowchart

3- Results and Discussion

The selected engine of this study was a four-stroke SI engine with injection inlet port valves. The engine is an in-line engine with 4 cylinders cooled by liquid water. The bore diameter is 150 mm, the piston stroke is 180 mm, and the nominal speed rate is 3000 rpm with a compression ratio of 15. The ambient condition of this study involved the atmospheric pressure of 1 bar and temperature of 288 K. This investigation is based on changing the compressor pressure ratio of the turbocharger from 2 to 10 at 2-bar intervals. The performance parameter of the engine was studied and recorded at each time the turbocharger compressor pressure ratio was changed.

Table 1 shows the parameters of the efficiency and power of the investigated engine with the different turbocharger compressor pressure ratios. The engine speed was fixed at 3000 rpm while the turbocharger compressor pressure ratios were varied from 2 to 10 bar. The piston engine power increased with enhancing the turbocharger compressor pressure ratio (TCPR) as well as the brake mean effective pressure and the brake torque. The previous values of the listed parameters were 603 *kW*, 18.95 bar, and 1919.6 *N.m* at the 2 TCPR and 2655.6 *kW*, 83.5 bar, and 8453.7 *N.m* at the 10 TCPR. Figure 4 shows the three types of engine efficiency: piston engine efficiency, indicated efficiency, and mechanical efficiency of the piston engine. The mechanical efficiency of the piston engine increased with the raising TCPR; while the indicated efficiency remained approximately constant. There was a slight increment in the efficiency of the piston engine with the increase of the TCPR. Overall the engine performance was affected by the increase of the TCPR.

Table 1. Parameters of efficiency and power

Efficiency and power parameters	Symbol	Turbocharger compressor pressure ratio				
		2	4	6	8	10
Engine Speed, rev/min	RPM	3000	3000	3000	3000	3000
Piston Engine Power, kW	P_eng	603	1151.6	1670.8	2171	2655.6
Brake Mean Effective Pressure, bar	BMEP	18.95	36.2	52.5	68.3	83.5
Brake Torque, N.m	Torque	1919.6	3665.8	5318.8	6912	8453.7
Mass of Fuel Supplied per cycle, g	m_f	0.44	0.83	1.19	1.54	1.87
Specific Fuel Consumption, kg/kWh	SFC	0.26	0.26	0.26	0.25	0.25
Specific Fuel Consumption in ISO, kg/kWh	SFC_ISO	0.27	0.27	0.26	0.26	0.26
Indicated Mean Effective Pressure, bar	IMEP	23.9	44.3	63.5	81.9	99.7
Mean Piston Speed, m/s	Sp	18	18	18	18	18
Friction Mean Effective Pressure, bar (Intern.Exp)	FMEP	3.84	6.22	8.5	10.7	12.8

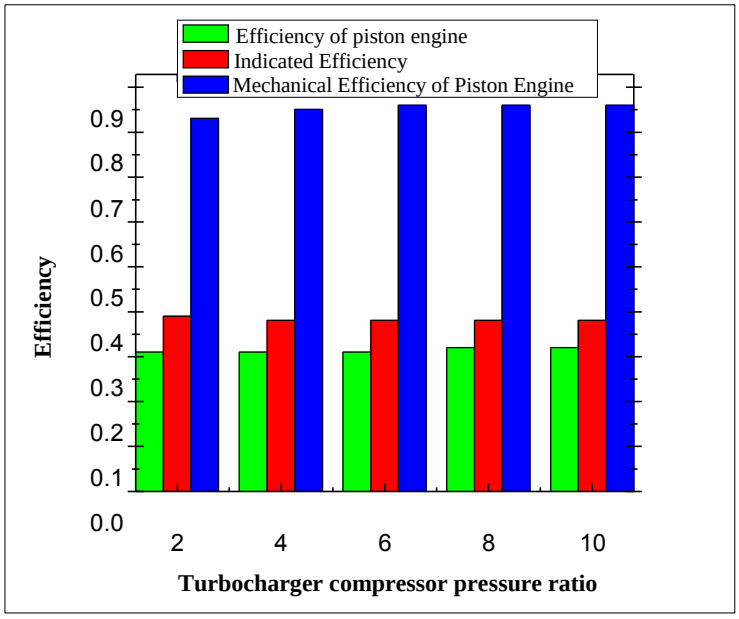

Figure 4. Engine efficiency

Table 2 presents the turbocharger and exchange parameters of the investigated engine. As seen, the volumetric efficiency of the turbocharger remained constant with the increase of the turbocharger compressor pressure ratio. The turbocharger efficiency, however, increased from 0.55 for 2 TCPR to 0.6 for 10 TCPR. The total air-fuel equivalence ratio and the total fuel-air equivalence ratio remained unchanged with the increase of the TCPR as well as the coefficient of the scavenging and the burnt gas fraction backflow into the intake percent. Figure 5 depicts the pressure of the turbocharger before the inlet manifold and the average total turbine inlet pressure. Both the mentioned pressures increased with the enhancing the TCPR. But, the pressure before the manifold showed a sharp increment with the increase of the TCPR. The engine performance was affected by increasing the TCPR as the engine temperature was elevated from 309.3 ℃ to 375.7 ℃ with the increase of the TCPR from 2 to 10 bar. The temperature elevation raised the total mass airflow to the piston from 0.66 to 2.8 m-air when the TCPR rose. The scavenging coefficient remained constant with increasing the TCPR as well as the total air-fuel equivalence of piston engine and the total fuel-air equivalence ratio.

Table 2. Turbocharger and exchange parameters

Turbocharging and gas exchange	Symbol	Turbocharger compressor pressure ratio				
		2	4	6	8	10
Temperature before Inlet Manifold, K	T_C	309.3	334.72	351.5	364.7	375.7
Total Mass Airflow (+EGR) of Piston Engine, kg/s	m_air	0.66	1.25	1.79	2.3	2.8
Turbocharger Efficiency	Eta_TC	0.55	0.57	0.58	0.59	0.6
Average Total Turbine Inlet Temperature, K	To_T	1040.5	1153.1	1214.4	1254.6	1285.1
Mass Exhaust Gasflow of Pison Engine, kg/s	m_gas	0.7	1.3	1.9	2.5	2.99
Total Air Fuel Equivalence Ratio (Lambda)	A/F_eq.t	1	1	1	1	1
Total Fuel Air Equivalence Ratio	F/A_eq.t	1	1	1	1	1
Pumping Mean Effective Pressure, bar	PMEP	-1.12	-1.9	-2.5	-2.99	-3.37
Volumetric Efficiency	Eta_v	0.99	0.99	1	1	1
Residual Gas Mass Fraction	x_r	0.017	0.014	0.012	0.012	0.01
Scavenging Coeff. (Delivery Ratio / Eta_v)	Phi	1	1	1	1	1
Burnt Gas Fraction Backflowed into the Intake, %	BF_int	0	0	0	0	0
% of Blow-by through piston rings	%Blow-by	0.097	0.1	0.1	0.1	0.1

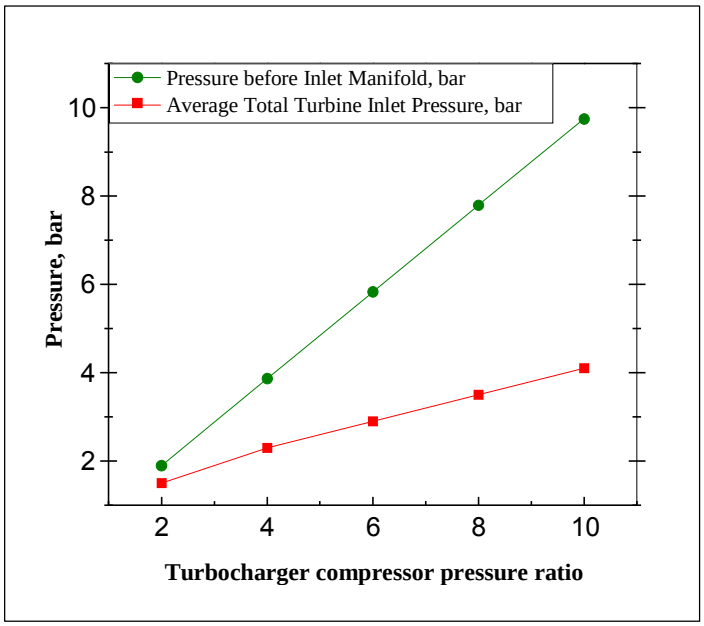

Figure 5. Pressure of the turbocharger before the manifold and the average total turbine inlet

Table 3 shows the intake and exhaust parameters of the investigated engine. The average exhaust manifold temperature was higher than the average intake manifold temperature. Both of them rose with increasing the TCPR. The average gas velocity at the exhaust was higher than the intake stroke; both of which incremented with the increase of the TCPR. The rest of the exhaust parameters were higher than the intake stroke and all increased with the elevation of the TCPR. The only opposing parameter was the total effective valve port throat area which was higher in the intake stroke as compared with the exhaust stroke. It, however, rose with the increase of the TCPR. Figure 6 shows the average manifold pressure of the intake and exhaust strokes. Accordingly, the average manifold pressure of the intake stroke was higher than the average pressure of the average exhaust manifold pressure and both of them increased with the increment of the TCPR. The results of the intake system show that the total effective valve port throat area remained constant with the increase of the TCPR; the same trend held for the max velocity in the middle section of the inlet port and the average gas velocity. The rest of the parameters exhibited an incremental pattern with increasing the TCPR.

Table 3. Intake and exhaust parameters

Intake system	symbol	Turbocharger compressor pressure ratio				
		2	4	6	8	10
Average Intake Manifold Temperature, K	T_int	312.85	338.15	354.99	368.2	379.3
Average Gas Velocity in intake manifold, m/s	v_int	44.4	44.8	44.8	44.88	44.9
Average Intake Manifold Wall Temperature, K	Tw_int	362.85	388.15	404.99	418.2	429.3
Heat Transfer Coeff. in Intake Manifold, W/(m^2*K)	hc_int	156.55	234.89	295.3	346.1	390.99
Heat Transfer Coeff. in Intake Port, W/(m^2*K)	hc_int.p	313.66	291.91	280.3	272.5	266.8
Max Velocity in a Middle Section of Int. Port, m/s	v_int.p	90.65	90.23	90	89.99	90
Total Effective Valve Port Throat Area, cm^2	A_v.thrt	25	25	25	25	25
Exhaust System						
Average Exhaust Manifold Gas Temperature, K	T_exh	1033.4	1138.4	1192.7	1227.2	1253.9
Average Gas Velocity in exhaust manifold, m/s	v_exh	141.02	203.3	246.05	275.8	294.88
Strouhal number: Sh=a*Tau/L (has to be: Sh > 8)	Sh	17.2	18.11	18.5	18.8	19
Average Exhaust Manifold Wall Temperature, K	Tw_exh	945.64	1049.9	1104.4	1139.4	1164.3
Heat Transfer Coeff. in Exhaust Manifold, W/(m^2*K)	hc_exh	299.67	376.07	424.3	451.5	465.95
Heat Transfer Coeff. in Exhaust Port, W/(m^2*K)	hc_exh.p	1378.5	1729.9	1951.8	2076.8	2143.4
Max Velocity in a Middle Section of Exh. Port, m/s	v_exh.p	186.5	192.2	195.4	197.6	199.19
Total Effective Valve Port Throat Area, cm^2	A_v.thrt	19.3	19.3	19.3	19.3	19.3

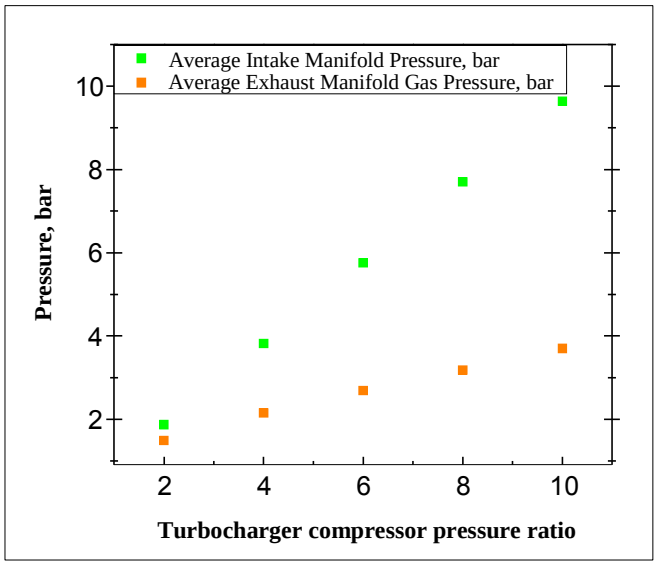

Figure 6. Intake and exhaust average manifold pressure

Figure 7 shows the NOx emission of the investigated engine due to the increase of the TCPR. Both NOx emissions (as a fraction of wet NOx in the exhaust gas and specific NOx emission) were reduced to NO by increasing the TCPR; implying the prominent role of TCPR in enhancing the NOx emissions of the engine, causing a positive effect on the environment.

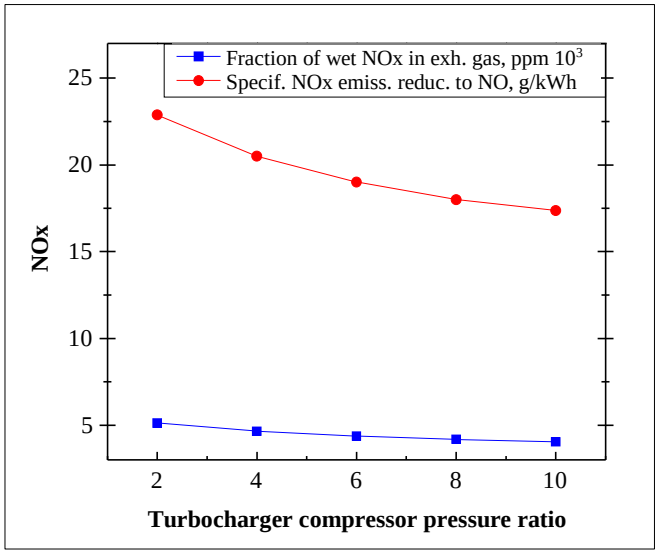

Figure 7. NOx emissions for the engine

Table 4 shows the parameters of the combustion and the heat exchange in the engine cylinder. As TCPR was increased, the air-fuel and fuel-air ratios remained constant during the combustion process. The combustion pressure and the temperature increased by enhancing the TCPR. The ignition timing, as well as the combustion duration, also remained constant during the combustion process as the TCPR was incremented. The rest of the combustion process parameters rose with elevating TCPR. The heat exchange in the engine cylinder was enhanced by the increase of the TCPR. Based on the enhancement of all the heat exchange parameters in Table. 4, the Boiling *Temp.* in Liquid Cooling System and Average Factor of Heat Transfer from head cooled surface to coolant remained constant when TCPR was enhanced in the heat exchange process.

Table 5 lists the compressor parameters of the studied engine. The parameters showed an enhancement in the engine's performance upon increasing the TCPR. Noteworthy, the adiabatic efficiency of the high-pressure compressor, the thermal efficiency of the high-pressure air inter-cooler, and the inlet total temperature of the high-pressure compressor remained constant by increasing the TCPR.

Table 4. Combustion and heat exchange parameters

Combustion	Symbol	Turbocharger compressor pressure ratio				
		2	4	6	8	10
Air Fuel Equival. Ratio (Lambda) in the Cylinder	A/F_eq	1	1	1	1	1
Fuel Air Equivalence Ratio in the Cylinder	F/A_eq	1	1	1	1	1
Maximum Cylinder Pressure, bar	p_max	269.7	540.52	796.25	1041.3	1278.5
Maximum Cylinder Temperature, K	T_max	3004.6	3151.4	3226.5	3274.4	3307.9
Angle of Max. Cylinder Pressure, deg. A.TDC	CA_p.max	2	1	1	1	1
Angle of Max. Cylinder Temperature, deg. A.TDC	CA_t.max	5	3	2	2	1
Max. Rate of Pressure Rise, bar/deg.	dp/dTheta	11.47	22.16	32.36	43.64	54.55
Ringing / Knock Intensity, MW/m^2	Ring_Intn	15.68	29.91	43.79	61.34	78.47
Max. Gas Force acting on the piston, kg	F_max	48282	96759	142539	186413	228871
Start Of Injection or Ignition Timing, deg. B.TDC	SOI	25	25	25	25	25
Ignition Delay Period, deg.	Phi_ign	0.15	0.15	0.15	0.15	0.15
Start of Combustion, deg. B.TDC	SOC	24.8	24.84	24.84	24.84	24.84
Combustion duration, deg.	Phi_z	44	44	44	44	44
Wiebe's Factor in the Cylinder	m_w	0.97	0.51	0.36	0.27	0.23
Minimum Octane Number of fuel (knock limit)	ON	204.9	302.68	373.75	431.6	481.29
HEAT EXCHANGE IN THE CYLINDER						
Average Equivalent Temperature of Cycle, K	T_eq	1788.2	1936.5	2007.7	2052	2082.4
Aver. Factor of Heat Transfer in Cyl., $W/m^2/K$	hc_c	1937.6	3379.4	4609.7	5715.4	6735.5
Average Piston Crown Temperature, K	Tw_pist	759.17	992.59	1150.7	1268.2	1360.2
Average Cylinder Liner Temperature, K	Tw_liner	413	413	413	413	413
Average Head Wall Temperature, K	Tw_head	703.06	919.06	1065.5	1174.3	1259.4
Average Temperature of Cooled Surface head of Cylinder Head, K	Tw_cool	534.58	644.35	718.03	773.52	816.3
Boiling Temp. in Liquid Cooling System, K	Tboil	386.65	386.65	386.65	386.65	386.65
Average Factor of Heat Transfer, $W/(m^2*K)$ from head cooled surface to coolant	hc_cool	12235	12235	12235	12235	12235
Heat Flow in a Cylinder Head, J/s	q_head	37156	60758	76754	88646	97950
Heat Flow in a Piston Crown, J/s	q_pist	35234	56365	69809	79156	85954
Heat Flow in a Cylinder Liner, J/s	q_liner	28720	53559	76380	97775	117991

Table 5. Compressor parameters

Compressor Parameters	Symbol	Turbocharger compressor pressure ratio				
		2	4	6	8	10
Rotor Speed of HPC, rev/min	RPM_C.hp	48333	77986	99040	111494	115350
Power of HPC, kW	P_C.hp	56.3	234.4	458.2	713.3	992
Adiabatic Efficiency of HPC	Eta_C.hp	0.74	0.75	0.76	0.76	0.76
Mass Airflow of HP Compressor, kg/s	m_C.hp	0.65	1.24	1.79	2.3	2.8
Mass Airflow Parameter, kg SQRT(K)/(s bar)	m*_C.hp	11.39	21.61	31	40	48.7
Corrected Mass Airflow of HPC, kg/s	m.cor_Chp	0.65	1.25	1.8	2.32	2.8
Rotor Speed Parameter, rev/min SQRT(K)	RPM*_C.hp	2848	4595.4	5836	6569.9	6797
Corrected Rotor Speed, rev/min	RPMcor_hp	49165	79328	100744	113413	117336
Inlet Total Pressure of HPC, bar	po_iC.hp	0.98	0.98	0.98	0.98	0.98
Inlet Total Temperature of HPC, K	To_iC.hp	288	288	288	288	288
Total Discharge Press. (before HP cooler), bar	po_"C.hp	1.96	3.9	5.88	7.84	9.8
Total Discharge Temp. (before HP cooler), K	To_"C.hp	373.24	474.87	541.9	594.7	638
Thermal Efficiency of HP Air Inter-cooler	Ecool.hp	0.75	0.75	0.75	0.75	0.75
HP Inter-cooler Refrigerant Temperature, K	Tcool.hp	288	288	288	288	288
Total Pressure after Inter-cooler, bar	po_C.hp	1.9	3.87	5.83	7.79	9.75
Total Temperature after Inter-cooler, K	To_C.hp	309.3	334.7	351.5	364.7	375.7

Based on the results, a rise in the turbocharger-supplied pressure ratio of the engine significantly enhanced the engine efficiency. There is congruence with a large group of researchers around the world. For example, Wang et al. (2022) [45] explored the effect and load demand of the Miller cycle based on using a low-speed marine engine and turbocharger and found that the use of a turbocharger with different designs and pressures can influence the engine performance. Lu et al. (2022) [46] conducted a parametric investigation into a marine diesel engine with a recirculation exhaust gas and turbocharger system. They expressed the major role of the recirculation and turbocharger systems in the performance of the engine. Other researchers shared the same idea about the use of the turbocharger to enhance engine performance [47-49].

4- Conclusion

This study was aimed at modifying the performance of the internal combustion engine by changing the turbocharger compressor pressure ratio and examining the parameters and criteria that can reverse the performance of the engine depending on the intake and exhaust strokes as well as the combustion with the heat transfer parameters. The findings revealed that all the performance parameters were positively affected by increasing the turbocharger compressor pressure ratio as the performance of the engine was enhanced by raising the TCPR. The turbocharger efficiency also exhibited an enhancement with the increase of the TCPR as it increased from 0.55 to 0.6 with the increase of the TCPR from 2 to 10. The pressure before the inlet manifold was enhanced from 2 to 10 bars with an equivalent increment in the TCPR. One of the important factors affected by the increase in TCPR is the emission of NOx as Wet NOx or NOx which is converted to NO. Both NOx types were decreased by the increasing TCPR. The thermal efficiency of the high-pressure air inlet cooler of the compressor remained constant (0.75) upon the increase of the TCPR. This study can contribute to enhancing the performance of the internal combustion engines by improving the engine design to face the new needs.

5- Declarations

5-1- Author Contributions

Conceptualization, S.S.A. and A.M.A.; methodology, T.K.M.; software, S.S.A.; validation, S.S.A., A.M.A. and T.K.M.; formal analysis, S.S.A.; investigation, S.S.A.; resources, A.M.A.; data curation, A.M.A.; writing—original draft preparation, S.S.A.; writing—review and editing, A.M.A.; visualization S.S.A.; supervision, S.S.A.; project administration, S.S.A.; funding acquisition, S.S.A. All authors have read and agreed to the published version of the manuscript.

5-2- Data Availability Statement

Data presented in this study are available in article.

5-3- Funding and Acknowledgements

I gratefully acknowledge the funding of the project (428/2021) by the deanship of academic research - Mutah University. This work is done by the researcher under Mutah University regulation and policy.

5-4- Conflicts of Interest

The authors declare that there is no conflict of interests regarding the publication of this manuscript. In addition, the ethical issues, including plagiarism, informed consent, misconduct, data fabrication and/or falsification, double publication and/or submission, and redundancies have been completely observed by the authors.

6- References

[1] Al-Najideen, M. I., & Alrwashdeh, S. S. (2017). Design of a solar photovoltaic system to cover the electricity demand for the faculty of Engineering- Mu'tah University in Jordan. Resource-Efficient Technologies, 3(4), 440–445. doi:10.1016/j.reffit.2017.04.005.

[2] Alrwashdeh, S. S. (2017). Determining the optimum tilt solar angle of a PV applications at different sites in Jordan. Journal of Engineering and Applied Sciences, 12(Specialissue11), 9295–9303. doi:10.3923/jeasci.2017.9295.9303.

[3] Tur, M. R., Colak, I., & Bayindir, R. (2018). Effect of Faults in Solar Panels on Production Rate and Efficiency. 2018 International Conference on Smart Grid (icSmartGrid). doi:10.1109/isgwcp.2018.8634509.

[4] Liu, T., Liu, Q., Lei, J., & Sui, J. (2019). A new solar hybrid clean fuel-fired distributed energy system with solar thermochemical conversion. Journal of Cleaner Production, 213, 1011–1023. doi:10.1016/j.jclepro.2018.12.193.

[5] Alrwashdeh, S. S. (2018). The effect of solar tower height on its energy output at Ma'an-Jordan. AIMS Energy, 6(6), 959–966. doi:10.3934/ENERGY.2018.6.959.

[6] Deshmukh, S. S., & Pearce, J. M. (2021). Electric vehicle charging potential from retail parking lot solar photovoltaic awnings. Renewable Energy, 169, 608–617. doi:10.1016/j.renene.2021.01.068.

[7] Alrwashdeh, S. S. (2018). Modelling of operating conditions of conduction heat transfer mode using energy 2D simulation. International Journal of Online Engineering, 14(9), 200–207. doi:10.3991/ijoe.v14i09.9116.

[8] Ghodbane, M., Boumeddane, B., Said, Z., & Bellos, E. (2019). A numerical simulation of a linear Fresnel solar reflector directed to produce steam for the power plant. Journal of Cleaner Production, 231, 494–508. doi:10.1016/j.jclepro.2019.05.201.

[9] Alrwashdeh, S. S. (2019). Investigation of Wind Energy Production at Different Sites in Jordan Using the Site Effectiveness Method. Energy Engineering: Journal of the Association of Energy Engineering, 116(1), 47–59. doi:10.1080/01998595.2019.12043338.

[10] Chiesi, M., Vanzolini, L., Franchi Scarselli, E., & Guerrieri, R. (2013). Accurate optical model for design and analysis of solar fields based on heterogeneous multicore systems. Renewable Energy, 55, 241–251. doi:10.1016/j.renene.2012.12.025.

[11] Osmani, K., Haddad, A., Lemenand, T., Castanier, B., & Ramadan, M. (2020). A review on maintenance strategies for PV systems. Science of the Total Environment, 746, 141753. doi:10.1016/j.scitotenv.2020.141753.

[12] Alrwashdeh, S. S. (2021). Investigation of the energy output from PV panels based on using different orientation systems in Amman-Jordan. Case Studies in Thermal Engineering, 28, 101580. doi:10.1016/j.csite.2021.101580.

[13] Hrayshat, E. S. (2007). Analysis of renewable energy situation in Jordan. Renewable and Sustainable Energy Reviews, 11(8), 1873–1887. doi:10.1016/j.rser.2006.01.003.

[14] Alrwashdeh, S. S., & Ammari, H. (2019). Life cycle cost analysis of two different refrigeration systems powered by solar energy. Case Studies in Thermal Engineering, 16. doi:10.1016/j.csite.2019.100559.

[15] Alrwashdeh, S. S., Markötter, H., Haußmann, J., Arlt, T., Klages, M., Scholta, J., Banhart, J., & Manke, I. (2016). Investigation of water transport dynamics in polymer electrolyte membrane fuel cells based on high porous micro porous layers. Energy, 102, 161–165. doi:10.1016/j.energy.2016.02.075.

[16] Alrwashdeh, S. S., Markötter, H., Haußmann, J., Scholta, J., Hilger, A., & Manke, I. (2016). X-ray Tomographic Investigation of Water Distribution in Polymer Electrolyte Membrane Fuel Cells with Different Gas Diffusion Media. ECS Transactions, 72(8), 99–106. doi:10.1149/07208.0099ecst.

[17] Göbel, M., Kirsch, S., Schwarze, L., Schmidt, L., Scholz, H., Haußmann, J., Klages, M., Scholta, J., Markötter, H., Alrwashdeh, S., Manke, I., & Müller, B. R. (2018). Transient limiting current measurements for characterization of gas diffusion layers. Journal of Power Sources, 402, 237–245. doi:10.1016/j.jpowsour.2018.09.003.

[18] Ince, U. U., Markötter, H., George, M. G., Liu, H., Ge, N., Lee, J., Alrwashdeh, S. S., Zeis, R., Messerschmidt, M., Scholta, J., Bazylak, A., & Manke, I. (2018). Effects of compression on water distribution in gas diffusion layer materials of PEMFC in a point injection device by means of synchrotron X-ray imaging. International Journal of Hydrogen Energy, 43(1), 391–406. doi:10.1016/j.ijhydene.2017.11.047.

[19] Markötter, H., Manke, I., Böll, J., Alrwashdeh, S., Hilger, A., Klages, M., Haussmann, J., & Scholta, J. (2019). Morphology correction technique for tomographic in-situ and operando studies in energy research. Journal of Power Sources, 414, 8–12. doi:10.1016/j.jpowsour.2018.12.072.

[20] Guermoui, M., Melgani, F., Gairaa, K., & Mekhalfi, M. L. (2020). A comprehensive review of hybrid models for solar radiation forecasting. Journal of Cleaner Production, 258, 120357. doi:10.1016/j.jclepro.2020.120357.

[21] Davlatshoevich, N. D. (2021). Investigation Optical Properties of the Orthorhombic System CsSnBr3-xIx: Application for Solar Cells and Optoelectronic Devices. Journal of Human, Earth, and Future, 2(4), 404–411. doi:10.28991/hef-2021-02-04-08.

[22] Alrwashdeh, S. S. (2018). Assessment of photovoltaic energy production at different locations in Jordan. International Journal of Renewable Energy Research, 8(2), 797–804.

[23] Alrwashdeh, S. S., Ammari, H., Madanat, M. A., & Ala'a, M. (2022). The Effect of Heat Exchanger Design on Heat transfer Rate and Temperature Distribution. Emerging Science Journal, 6(1), 128-137. doi:10.28991/ESJ-2022-06-01-010.

[24] Sabe'Alrwashdeh, S., Markötter, H., Haußmann, J., Scholta, J., Hilger, A., & Manke, I. (2016). X-ray tomographic investigation of water distribution in polymer electrolyte membrane fuel cells with different gas diffusion media. ECS Transactions, 72(8), 99. doi:10.1149/07208.0099ecst.

[25] Ammari, H. D., Al-Rwashdeh, S. S., & Al-Najideen, M. I. (2015). Evaluation of wind energy potential and electricity generation at five locations in Jordan. Sustainable Cities and Society, 15, 135–143. doi:10.1016/j.scs.2014.11.005.

[26] Gautam, S. S., Singh, R., Vibhuti, A. S., Sangwan, G., Mahanta, T. K., Gobinath, N., & Feroskhan, M. (2022). Thermal barrier coatings for internal combustion engines: A review. Materials Today: Proceedings, 51, 1554–1560. doi:10.1016/j.matpr.2021.10.371.

[27] Sinigaglia, T., Eduardo Santos Martins, M., & Cezar Mairesse Siluk, J. (2022). Technological evolution of internal combustion engine vehicle: A patent data analysis. Applied Energy, 306, 118003. doi:10.1016/j.apenergy.2021.118003.

[28] Catapano, F., Perozziello, C., & Vaglieco, B. M. (2021). Heat transfer of a Stirling engine for waste heat recovery application from internal combustion engines. Applied Thermal Engineering, 198, 117492. doi:10.1016/j.applthermaleng.2021.117492.

[29] Guo, C., Zuo, Z., Feng, H., & Roskilly, T. (2021). Advances in free-piston internal combustion engines: A comprehensive review. Applied Thermal Engineering, 189, 116679. doi:10.1016/j.applthermaleng.2021.116679.

[30] Gao, J., Wang, X., Song, P., Tian, G., & Ma, C. (2022). Review of the backfire occurrences and control strategies for port hydrogen injection internal combustion engines. Fuel, 307, 121553. doi:10.1016/j.fuel.2021.121553.

[31] Aliramezani, M., Koch, C. R., & Shahbakhti, M. (2022). Modeling, diagnostics, optimization, and control of internal combustion engines via modern machine learning techniques: A review and future directions. Progress in Energy and Combustion Science, 88, 100967. doi:10.1016/j.pecs.2021.100967.

[32] Cuenca, C. A., & Gonzaga-Bermeo, L. (2022). Structural design of the base of an internal combustion engine using FEM. Materials Today: Proceedings, 49, 135–141. doi:10.1016/j.matpr.2021.07.486.

[33] Novotny, V., Spale, J., Szucs, D. J., Tsai, H. Y., & Kolovratnik, M. (2021). Direct integration of an organic Rankine cycle into an internal combustion engine cooling system for comprehensive and simplified waste heat recovery. Energy Reports, 7, 644–656. doi:10.1016/j.egyr.2021.07.088.

[34] Omara, A. A. M. (2021). Phase change materials for waste heat recovery in internal combustion engines: A review. Journal of Energy Storage, 44, 103421. doi:10.1016/j.est.2021.103421.

[35] Jafari, H., Yang, W., & Ryu, C. (2020). Evaluation of a distributed combustion concept using 1-D modeling for pressurized oxy-combustion system with low flue gas recirculation. Fuel, 263, 116723. doi:10.1016/j.fuel.2019.116723.

[36] Negoro, A. B., & Purwadi, A. (2013). Performance Analysis on Power Train Drive System of the 2012 Toyota Camry Hybrid. Procedia Technology, 11, 1054–1064. doi:10.1016/j.protcy.2013.12.294.

[37] Doppalapudi, A. T., Azad, A. K., & Khan, M. M. K. (2021). Combustion chamber modifications to improve diesel engine performance and reduce emissions: A review. Renewable and Sustainable Energy Reviews, 152, 111683. doi:10.1016/j.rser.2021.111683.

[38] Mücková, P., Famfulík, J., & Richtár, M. (2021). Optimization of four stroke spark ignition engine for firesport. Transportation Research Procedia, 55, 496–502. doi:10.1016/j.trpro.2021.07.014.

[39] Yousefi, A., Guo, H., Dev, S., Liko, B., & Lafrance, S. (2022). Effects of ammonia energy fraction and diesel injection timing on combustion and emissions of an ammonia/diesel dual-fuel engine. Fuel, 314, 122723. doi:10.1016/j.fuel.2021.122723.

[40] Sykes, D., Turner, J., Stetsyuk, V., de Sercey, G., Gold, M., Pearson, R., & Crua, C. (2021). Quantitative characterisations of spray deposited liquid films and post-injection discharge on diesel injectors. Fuel, 289, 119833. doi:10.1016/j.fuel.2020.119833.

[41] Alrwashdeh, S. S., Alsaraireh, F. M., Saraireh, M. A., Markötter, H., Kardjilov, N., Klages, M., Scholta, J., & Manke, I. (2018). In-situ investigation of water distribution in polymer electrolyte membrane fuel cells using high-resolution neutron tomography with 6.5 μm pixel size. AIMS Energy, 6(4), 607–614. doi:10.3934/energy.2018.4.607.

[42] Zhang, T. (2022). An estimation method of the fuel mass injected in large injections in Common-Rail diesel engines based on system identification using artificial neural network. Fuel, 310, 122404. doi:10.1016/j.fuel.2021.122404.

[43] Lan, Q., Bai, Y., Fan, L., Gu, Y., Wen, L., & Yang, L. (2020). Investigation on fuel injection quantity of low-speed diesel engine fuel system based on response surface prediction model. Energy, 211, 118946. doi:10.1016/j.energy.2020.118946.

[44] Schifter, I., González-Macías, C., & Mejía-Centeno, I. (2022). Merit function for simultaneous optimization of fuel properties, naturally aspirated spark-ignition engines equipped with port fuel injection system, and regulated emissions. Fuel, 313, 122701. doi:10.1016/j.fuel.2021.122701.

[45] Wang, D., Shi, L., Zhang, H., Li, X., Qian, Y., & Deng, K. (2022). Research on influence and demand of Miller cycle based on the coupling of marine low-speed engine and turbocharger. Applied Thermal Engineering, 200, 117624. doi:10.1016/j.applthermaleng.2021.117624.

[46] Lu, D., Theotokatos, G., Zhang, J., Zeng, H., & Cui, K. (2022). Parametric investigation of a large marine two-stroke diesel engine equipped with exhaust gas recirculation and turbocharger cut out systems. Applied Thermal Engineering, 200, 117654. doi:10.1016/j.applthermaleng.2021.117654.

[47] Jung, I. D. (2021). Process and design optimization for powder injection molding of turbocharger vanes. Metal Powder Report, 76(5), 26–29. doi:10.1016/S0026-0657(21)00285-X.

[48] Peixoto, T. F., Nordmann, R., & Cavalca, K. L. (2021). Dynamic analysis of turbochargers with thermo-hydrodynamic lubrication bearings: Abstract. Journal of Sound and Vibration, 505, 116140. doi:10.1016/j.jsv.2021.116140.

[49] Novotný, P., Vacula, J., & Hrabovský, J. (2021). Solution strategy for increasing the efficiency of turbochargers by reducing energy losses in the lubrication system. Energy, 236, 121402. doi:10.1016/j.energy.2021.121402.